International Journal of Biological Macromolecules 150 (2020) 218–227

Contents lists available at ScienceDirect

International Journal of Biological Macromolecules

journal homepage: http://www.elsevier.com/locate/ijbiomac

Binding of pDNA with cDNA using hybridization strategy towards monitoring of Haemophilus influenza genome in human plasma samples

Arezoo Saadati [a,b], Soodabeh Hassanpour [c,d], Mohammad Hasanzadeh [e,*], Nasrin Shadjou [f,*]

[a] Food and Drugs Safety Research Center, Tabriz University of Medical Science, Tabriz, Iran
[b] Biotechnology Research Center, Tabriz University of Medical Sciences, Tabriz, Iran
[c] Nutrition Research Center, Tabriz University of Medical Science, Tabriz, Iran
[d] Department of Analytical Chemistry, Faculty of Science, Palacky University Olomouc, 17, listopadu 12, 77146 Olomouc, Czech Republic
[e] Pharmaceutical Analysis Research Center, Tabriz University of Medical Sciences, Tabriz, Iran
[f] Department of Nanotechnology, Faculty of Science and Chemistry, Urmia University, Urmia, Iran

ARTICLE INFO

Article history:
Received 16 December 2019
Received in revised form 1 February 2020
Accepted 7 February 2020
Available online 10 February 2020

Keywords:
DNA hybridization
Bioassay
Nucleic acid binding
Silver nanoparticles
Haemophilus influenza

ABSTRACT

Haemophilus Influenza leads to respiratory infections such as sinusitis, acute otitis media, pneumonia and bronchitis. In addition, it causes invasive infections such as cellulite, septic arthritis, and meningitis. Therefore, quick and sensitive detection of H. influenza is of great importance in medical microbiology. In this study, a novel DNA-based bioassay was developed to the monitoring of *Haemophilus influenza* genome in human plasma samples using binding of pDNA with cDNA. DNA hybridization strategy was used to investigation of DNAs binding. For this purpose, silver nanoparticle doped graphene quantum dots inks functionalized by D-penicillamine (Ag NPs-DPA-GQDs) were synthesized and deposited on the surface of glass carbon electrode (GCE). Also, gold nanoparticles functionalized with cysteamine (CysA-AuNPs) were deposited on the surface of the Ag-DPA-GQDs modified GCE. Afterward, thiolated DNA probe was immobilized on the surface of the modified electrode. DNA hybridization was monitored using square wave voltammetry (SWV) technique. Engineered genosensor indicated good performance with high specificity and sensitivity for detection of *Haemophilus influenza* genome. Under optimal conditions, linear range and low limit of quantitation (LLOQ) were obtained as target concentrations ranging from 1 pM–1 ZM and 1 ZM, respectively. The designed biosensor also showed high capability of discriminating one-base, two-base and three-base mismatched sequences. Also, the prepared genosensor could be easily regenerated and reused to evaluate hybridization process.

1. Introduction

The use of electrochemical methods for DNA hybridization was first proposed by Millan and Mikkelsen [1]. Subsequently, DNA-based electrochemical biosensors were used to diagnose various types of infectious diseases such as *E. coli* infection [2], Vibrio cholera, Foodborne disease [3], syphilis [4], Salmonella infection, HIV Aids [5], leptospirosis [6], Tuberculosis [7], dengue fever [8], and influenza [9]. *Haemophilus influenza*, a gram negative coccobacillus that classifies by producing polysaccharide capsules. Nontypeable strains do not produce any capsules. Capsulated strains are classified into 6 serotypes A to F according to the kind of capsular antigen [10]. The capsule provides resistance to the complement system and phagocytosis, so non-capsulated strains have less invasive attributes [11]. *H. influenza* leads to respiratory infections such as sinusitis, acute otitis media, pneumonia and bronchitis. In addition, it causes invasive infections such as cellulite, septic arthritis, and meningitis [12]. Therefore, quick and sensitive detection of H. influenza is of great importance in medical microbiology. There are several methods to diagnose H. influenza, including culture, LAT (latex particle agglutination), and PCR (Polymerase chain reaction). The culture and LAT methods are commonly used for the clinical diagnosis of the virus [13,14]. But, since the *H. influenza* is a fastidious bacterium, growing it requires complex nutrition. Also, replication of these viruses is time-consuming and may take several days or weeks. PRC is more sensitive and specific than previous methods, but it also has disadvantages [15]. Therefore, due to the disadvantages of old methods such as time-consuming, low specificity and sensitivity, the need for specialized people, advanced and expensive equipment, new methods including biosensors have been developed for virus detection [16]. Genosensors and immunosensors are commonly used to detect infectious diseases [17,18]. In the case of DNA-based electrochemical sensors, an important analytical parameter in the detection of DNA hybridization is the electrochemical

* Corresponding authors.
E-mail addresses: hasanzadehm@tbzmed.ac.ir (M. Hasanzadeh), n.shadjou@urmia.ac.ir (N. Shadjou).

https://doi.org/10.1016/j.ijbiomac.2020.02.062
0141-8130/

signal change in the presence and absence of target DNA [19]. There are various methods such as voltammetry, amperometric, conductometric, and potentiometric to measure the electrochemical signal of DNA hybridization [20].

In recent years, DNA-based biosensors have been extensively used for their specificity, high sensitivity, simplicity, low cost and minimization capability [21]. DNA hybridization is the most important principle in the preparation of DNA-based electrochemical biosensors, which includes single-stranded DNA (ssDNA) immobilization on the electrode surface and target DNA detectability for double-stranded helix formation [22,23]. Because of the simplicity and direct conversion of the hybridization process to the electrical signal, electrochemical transducers have received much attention in the detection of DNA hybridization [24,25]. With the advent of nanotechnology, different types of nanoparticles and conductive nano-inks are used to immobilize the thiolated DNA probe owing to their exceptional properties such as biocompatibility, high surface area and high adsorption power. On the other hand, Au NPs (gold nanoparticles), as conductive mediators, are capable of enhancing the electrical response through electrochemical signal transduction and can also maintain their biological activity. Hence, Au NPs are used for DNA probe immobilization on the electrode surface. In addition, gold is able to form a strong bond with molecules containing thiols such as cysteamine, mercaptopropionic acid, and mercaptosuccinic acid [21]. Different types of conductive inks such as conductive polymers, nanoparticle inks and metallic inks are employed for the preparation of electrochemical sensors. Silver nanoparticles due to their high electrical conductivity, optical and thermal properties lead to differentiation in conductive inks containing Ag compared to other inks. Zero-dimensional graphene quantum dot nanocrystals are widely used in electrochemical sensors due to their lower toxicity, water solubility, cheap and extensive resources, biocompatibility and chemical inactivity [26–31]. Given the benefits of graphene quantum dot based nanocomposites in the development of bio-devices for DNA hybridization monitoring, this work presented the engineered genosensor using Ag-DPA-GQDs conductive nano-inks to detection of H. influenza in human plasma samples. To prepare the desired genosensor, Ag-DPA-GQDs ink was synthesized and deposited on the surface of the GCE. Then, gold nanoparticles functionalized by cysteamine were deposited on the surface of Ag-DPA-GQDs modified GCE and the ssDNA primer was immobilized on the surface of the substrate. Finally, DNA hybridization and interaction of ssDNA-dsDNA was evaluated by square wave voltammetry (SWV) technique.

2. Materials and methods

2.1. Chemicals and reagents

Sodium acetate (CH_3COONa), D-penicillamine (DPA), hydrogen tetrachloroaurate (III) hydrate ($HAuCl_4.3H_2O$), citric acid, potassium chloride (KCl), sodium hydroxide (NaOH), potassium ferrocyanide $K_4Fe(CN)_6$, potassium ferrocyanide $K_3Fe(CN)_6$, TB (toluidine blue), DTT (Dithiotrietol), MCE (mercaptoethanol), and polyvinyl pyrrolidone (PVP) K-30 were purchased from Sigma-Aldrich (Ontario, Canada). The oligonucleotide sequences achieved from Takapouzist Co. (Iran) include:

- Probe single strand DNA(ssDNA): SH-5′-AAT TTT CCA ACT TTT TCA CCT GCA T-3′
- Complementary target DNA: 5′-ATG CAG GTG AAA AAG TTG GAA AAT T-3′
- 1-Base mismatched target DNA: 5′-ATG GAG GTG AAA AAG TTG GAA AAT T-3′
- 2-Base mismatched target DNA: 5′-AGG GAG GTG AAA AAG TTG GAA AAT T-3′
- 3-Base mismatched target DNA: 5′-AGG GAG GTG AGA AAG TTG GAA AAT T-3′

Dilution of oligonucleotides was performed using Tris-HCl buffer (0.1 M, pH~7.4). DTT solution was made ready using 500 mM DTT and 10 mM sodium acetate (pH~5.2). TB stock solution (20 μM) was applied as a redox marker to reveal DNA hybridization. Electrochemical studies were carried out using supporting electrolyte containing 0.5 mM $K_4Fe(CN)_6/K_3Fe(CN)_6$ (1:1) and 0.5 mM of KCl.

2.2. Apparatus

PalmSense 4c system (Palm instruments, Utrecht, The Netherlands) and unexceptional three-electrode (from Metrohm) were applied for electrochemical studies. Ag/AgCl-Sat'd KCl and platinum wire were applied as reference and counter electrode, respectively. The GCE (glass carbon electrode) with 2 mm in diameter (from Azar Electrode Co., Urumia, Iran) was also applied as a working electrode. Electrochemical system was run with PSTrace 5.3 software. Transmission electron microscopy (TEM) was carried out on a Philips CM30 electron microscope operated at 200 kV (Adelaide, Australia). Field emission scanning electron microscope (FE-SEM) (Hitachi-SU8020, Czech) with an operating voltage of 3 kV was performed to appraise the modified electrode surface and particles morphology. Atomic force microscopic (AFM) image was obtained on a Multimode 8 force microscope (Bruker, Germany). The chemical composition of the modified electrodes was investigated using energy dispersive spectroscopy (EDS). Dynamic light scattering (DLS) was evaluated using zeta potential instrument Malvern Instruments Ltd. (Zetasizer Ver. 7.11, MAL1032660, England) for size distribution and zeta potential. Square wave voltammetry (SWV) evaluations was performed using $E_{pulse} = 0.005$ V, pulse amplitude = 0.001 V, and frequency = 10.0 Hz.

2.3. Synthesis

2.3.1. Synthesis of CysA-AuNPs

Briefly, 5 mL of sodium citrate solution (38.8 mM) was added to 50 mL of magnetically stirred and boiled $HAuCl_4$ (0.5 mM). By adding sodium citrate, color of solution was changed from yellow to wine-red which stirring is continued until the color is fixed. Afterwards, the citrate capped-Au nanoparticles were functionalized using Cys A and its morphology was investigated [31].

2.3.2. Synthesis of graphene quantum dots doped by D-penicillamine (DPA-GQDs)

DPA-GQDs was synthesized using thermal pyrolysis of the mixture of D-penicillamine and citric acid. For this purpose, D-penicillamine was first extracted from the capsules using acetone and purified at room temperature. Then, the mixture obtained by dissolving D-penicillamine (0.29 g) and citric acid (0.95 g) in water (10 mL) and transferred to pressurized autoclave vessel. So, the solution was heated at 200 °C for 2.5 h.

2.3.3. Synthesis of silver nanoparticles deposited on the DPA-GQDs nano-ink

In order to synthesize the nano-ink, initially 0.6 g of graphite, 0.4 g of PVP K-30, and DPA-GQDs solution were mixed and magnetically stirred. Then, 0.2 M of $AgNO_3$ aqueous solution was added into the beginning solution and magnetically stirred. Afterwards, the mixture was incubated at 60 °C. After 12 h, the solution was magnetically stirred at 80 °C. Eventually, 2 M of NaOH solution was added dropwise to the solution. The outcome solution was centrifuged (30 min at 8000 rpm) and washed 3 times. In order to synthesize of hybrid conductive nano-ink, Ag-DPA-GQDs nano-ink were

dispersed into DI water, ethanol, and ethylene glycol with volume ratio of 9:9:3 and sonicated for 30 min.

2.4. Analysis of Ag-DPA-GQDs nano-ink conductivity

For this purpose, the conductivity of Ag-DPA-GQDs nano-composite was first measured using a conductometer (about 290 μs) and then, diverse conductive path were drawn on different surfaces including photographic paper, leaf, and electronic board using synthesized nano-ink. A dip LED (with a rated voltage of 1.5 V), the various conductive patterns and 1.5 V battery fixed on substrate are presented in Fig. 1 (see Supporting data for video files). Cathode legs of LED were linked to battery anode and so cathode surface of battery fixed to one side of conductive pattern. Once the anode leg of LED touched to other side of conductive pattern, the electronic circuit switched on and the LED was lighted up. At last, the resistance of conductive patterns was measured using conventional ohmmeter.

2.5. Construction of the electrochemical genosensor

To prepare the genosensor, GCE was polished to a mirror-like finish with 0.05 μm alumina slurry (Beuhler, USA) followed by washing thoroughly with double distilled water (DW). Then, it was consecutively sonicated in DW and acetone 1:1 (v/v) and allowed to dry. At the first step of the electrode modification, the Ag-DPA-GQDs nano-ink was transferred to the electrochemical cell and electrodeposition was performed using a cyclic voltammetry (CV) technique with 30 repetitive cycles in the potential range from −1 to 1 V and scan rate of 50 mV/s (Fig. 2A). Subsequently, CysA-Au NPs was electrodeposited on the surface of the Ag-DPA-GQDs nano-ink modified GCE by chronoamperometry technique at E = 0.0 V and duration time of 500 s (Fig. 2B). As shown in Fig. 2A, an anodic peak at 0.9 V and a reduction peak at −0.6 V were appeared to represent the formation of Ag-DPA-GQDs film on the surface of GCE. The results indicate that the Ag-DPA-GQDs film is formed by bonding between carbon and amino groups on the electrode surface.

For the preparation of DNA-based biosensor, pDNA probe combined with DTT and immobilized on the surface of the designed platform. Given that the pDNA has been modified with -SH (thiol) groups, DTT was used to prevent the formation of inter-molecular and intra-molecular disulfide bonds between proteins and cysteine residues and reduce protein disulfide bonds. Since, DTT cannot reduce embedded disulfide bonds, so their reduction is sometimes performed in the presence of denaturing agents or high temperatures [32,33]. In order to, sodium acetate and DTT solution were prepared and mixed with probe 1:1 (v/v) and preserved at room temperature for 30 min. Then, the solution was casted to the Ag-DPA-GQD/CysA-Au NP/GCE surface and incubated at 4 °C for 4 h. After washing the

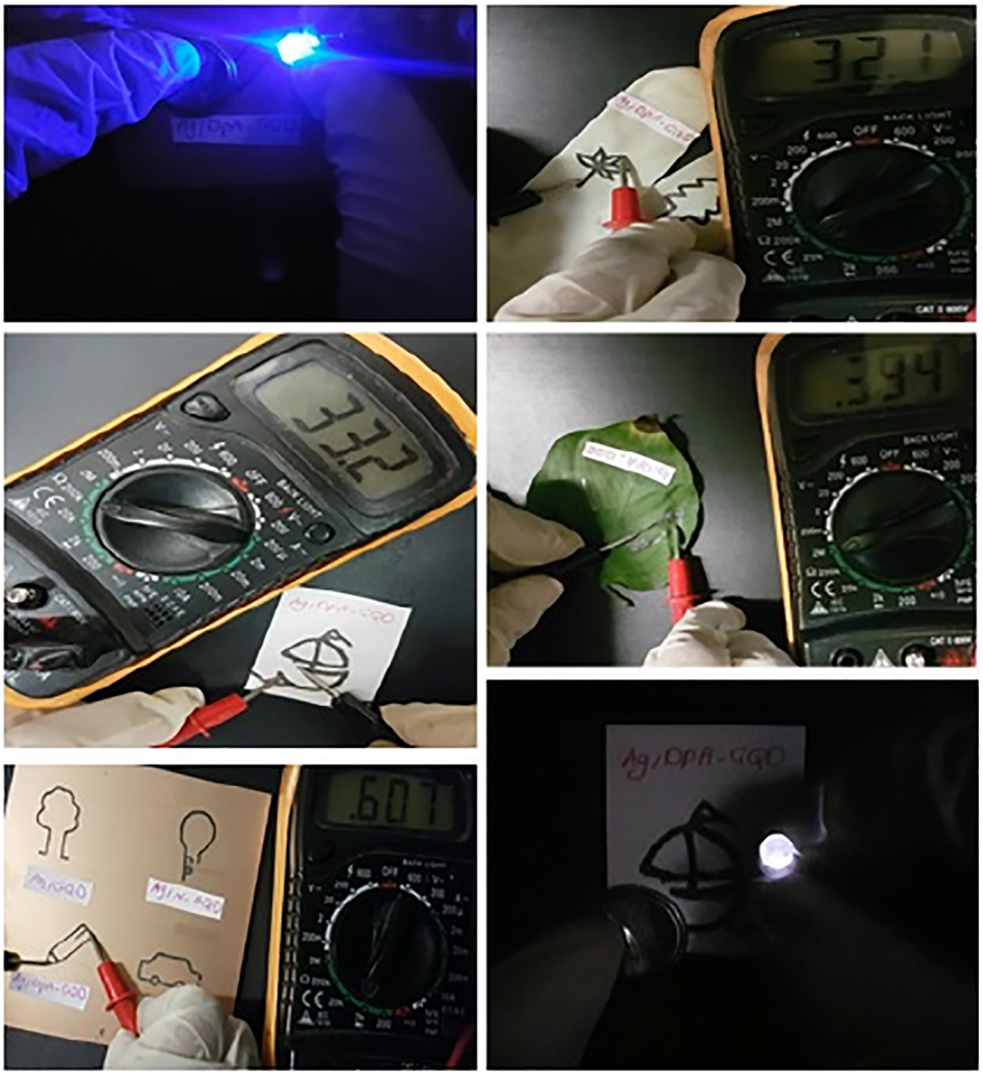

Fig. 1. Photographic images of diverse patterns obtained by Ag-DPA-GQD nano-ink on different substrate.

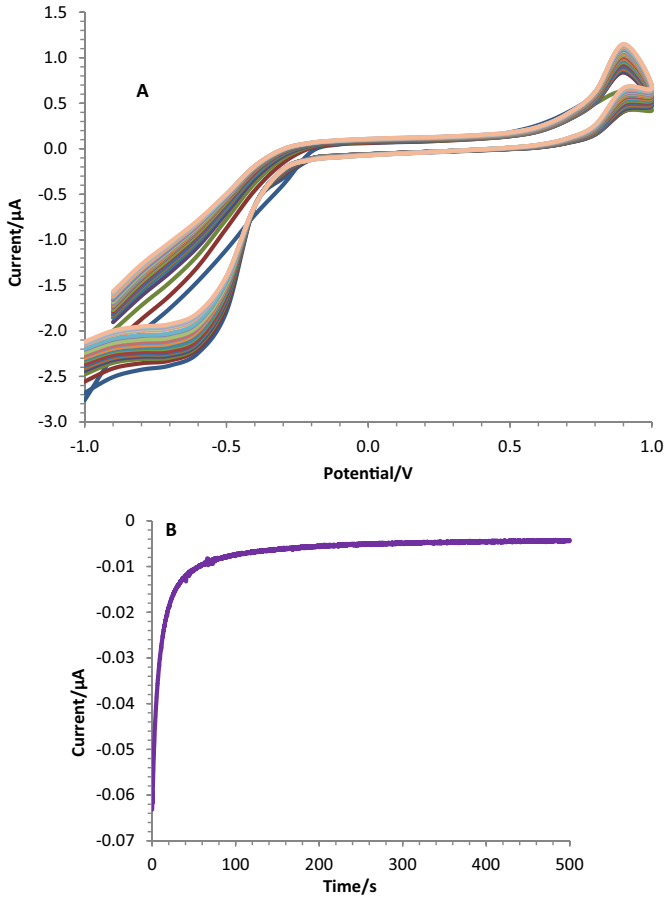

Fig. 2. (A) Repetitive CVs of GCE in the presence of Ag-DPA-GQDs nano-ink (scan rate = 50 mV/s, number of cycle = 30, potential range = −1 to +1 V). (B) Chronoamperogram of Ag-DPA-GQDs-GCE in the presence of CysA-Au NPs.

electrode with deionized water, pDNA modified sensor was incubated by MCE (mercaptoethanol) for 30 min at room temperature. MCE as a biological antioxidant results in blockage of unreacted sites and significant increase in DNA occupancy in the next step [34]. Subsequently, the TB (toluidine blue) solution was casted on the electrode surface to label the DNA probe. TB is basic thiazine metachromatic dye. Because of its high affinity for acidic tissues components, dyes tissues containing DNA and RNA. TB can be used as indicator in the redox systems [9]. The fabrication procedure of electrochemical genosensor was shown in Scheme 1.

3. Results and discussion

3.1. Characterizations

3.1.1. FE-SEM characterization

The surface morphology of the bulk Ag-DPA-GQDs nano-ink, Ag-DPA-GQD electrodeposited on GCE, CysA-Au NPs electrodeposited on Ag-DPA-GQDs/GCE, DNA probe casted on CysA-AuNPs/Ag-DPA-GQDs/GCE, and cDNA casted on pDNA/CysA-AuNPs/Ag-DPA-GQDs/GCE was evaluated using high resolution field emission scanning electron microscope (FE-SEM). The FE-SEM images of the various steps of the genosensor design and the bulk nano-ink are presented in Fig. 3. As shown in Fig. 3A, small silver nanoparticles with a uniform spherical structure was presented in DPA-GQDs. According to the standard theory of colloids, the stability of colloids depends on the equilibrium between the van der Waals interaction and the coulombic repulsion of the charged particles [35]. Conductivity in the PVP graphitic Ag-DPA-GQDs nano-ink also changes remarkably due to the anchoring of Ag NPs onto DPA-GQDs. The FE-SEM images of Ag-DPA-GQDs electrodeposited on the surface of GCE, demonstrated a regular structure (Fig. 3B). Fig. 3C shows also the distribution of Ag-DPA-GQDs/CysA-Au NPs on the surface of GCE resulting from the interaction between the amine and thiol functional groups. These results show that GCE has been successfully covered by Ag-DPA-GQDs/CysA-Au NPs film and can be useful for DNA probe immobilization. Finally, by adding cDNA to the surface of modified electrode, hybridization was investigated and the results showed that cDNA was successfully attached to the pDNA. It is important to point out that, high distribution of Ag-DPA-GQDs/CysA-Au NPs on the surface of GCE lead to increment on the dense-loading of pDNA. Therefore, high amount of pDNA is able to interact with cDNA which lead to better hybridization and increment of the sensitivity of the constructed genosensor.

As noticeable in Fig. S1 (see Supporting information), the signals of the Ag element belong to the nano-ink and Au to the CysA-Au NPs, while the carbon and nitrogen elements are both to the nano-ink and to the CysA-Au NPs. Large and sharp peaks from C and N appear due to the presence of carbon and nitrogen elements in the bulk of nano-ink. Another reason for the high and sharp carbon peak is due to the presence of graphite in the nano-ink formulation. The results also show that the elements C, N, and O overlap. Also, the appearance of O and P peak in the genosensor indicates the appropriate immobilization of DNA on the surface.

3.1.2. TEM characterization

The mechanism of Ag-DPA-GQDs nano-composite formation and evaluation of bonding of Ag and DPA-GQDs nanoparticles onto graphite sheets was investigated using TEM. TEM images recorded using the holey carbon grid which are shown in Fig. 4. By adding Ag NPs into the nano-ink mixture, an abundance of crystalline nuclei immediately forms. PVP as a protective and mildly reluctant, is immediately absorbed into the nuclei and prevents merger and aggregation of it.

3.1.3. AFM, FTIR, and DLS characterizations

Characterization of synthesized DPA-GQDs was performed using AFM, FTIR, and DLS. The AFM images and roughness analysis of GQD and DPA-GQDs were presented in Fig. S2 (see Supporting information) and Table 1. Given that, 90% of GQDs show a dark brown and range in size below 10 nm, which GQDs have a narrow monolayer structure. Also, synthesized DPA-GQDs has a thickness of 10 nm and contains a large amount of DPAs which are mainly attached to the edges of the GQDs.

The FTIR (Fourier transform infrared spectroscopy) results of GQDs and DPA-GQDs were shown in Fig. S3 (see Supporting information) which indicated the existence of the SH_3 stretching signal and N—H stretching signal in DPA-GQDs. In addition, the different type of the functionalized groups indicates the presence of amine groups such as $-NH_2$.

DLS analysis of DPA-GQDs shows two-dimensional sheet shape and low aggregation. Also, the average particle size for DPA-GQDs was 1.11 nm (Fig. S4 (see Supporting information)).

3.2. Electrochemical behavior

DNA hybridization is usually electrochemically detected by different behavior in the presence or absence of the target cDNA. The rate of hybridization is determined by electrochemical signal after hybridization with DNA probes tagged with nanoparticles or enzymes and redox peak current for hybridization indicator or electroactive DNA bases. Electrochemical behavior of electrode modification steps was evaluated by CV technique in $[Fe(CN)_6]^{3-/4-}$ solution. As shown in Fig. 5, bare GCE, GCE modified with (Ag-DPA-GQDs/GCE), Ag-DPA-GQDs/GCE modified with CysA/Au NPs (CysA-Au NPs/Ag-DPA-GQDs/GCE), GCE modified with pDNA (TB/pDNA/CysA-Au NPs/Ag-DPA-GQDs/GCE), GCE modified with cDNA (cDNA/TB/pDNA/CysA-Au NPs/Ag-DPA-

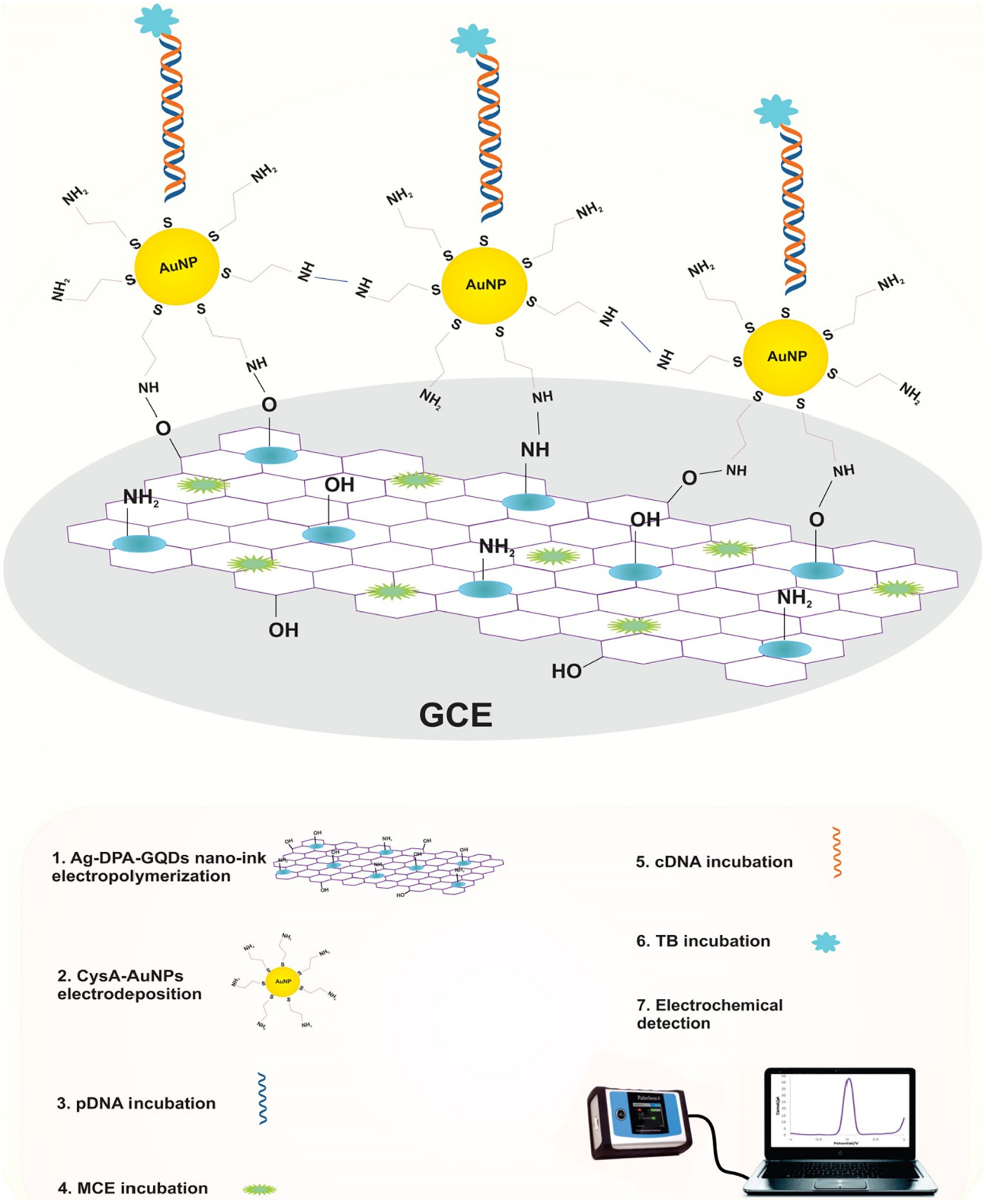

Scheme 1. The schematic illustration of the CysA-Au NPs modified Ag-DPA-GQDs nano-ink electrochemical genosensor for the detection of Haemophilus influenza.

GQDs/GCE) have different electrochemical behavior in terms of peak potential and current. The recorded voltammogram prior to modification showed current 50.42 at 0.3 V. After modification using Ag-DPA-GQDs nano-ink, oxidation peak with current 43.89 at potential 0.7 V was observed. This indicates that the conductive nano-ink reduces the electron transfer at the surface. Here, conductive nao-ink provides a suitable substrate for anchoring CysA-Au NPs. After electrodeposition of CysA-Au NPs, the peak current decreased to 44.11 μA and peak potential was 0.5 V. Gold nanoparticles functionalized with cysteamine provide a good surface for primer immobilization. After immobilization of the pDNA, no significant change in current is observed but the peak potential is changed to 0.2 V. After biosensor preparation, cDNA is added

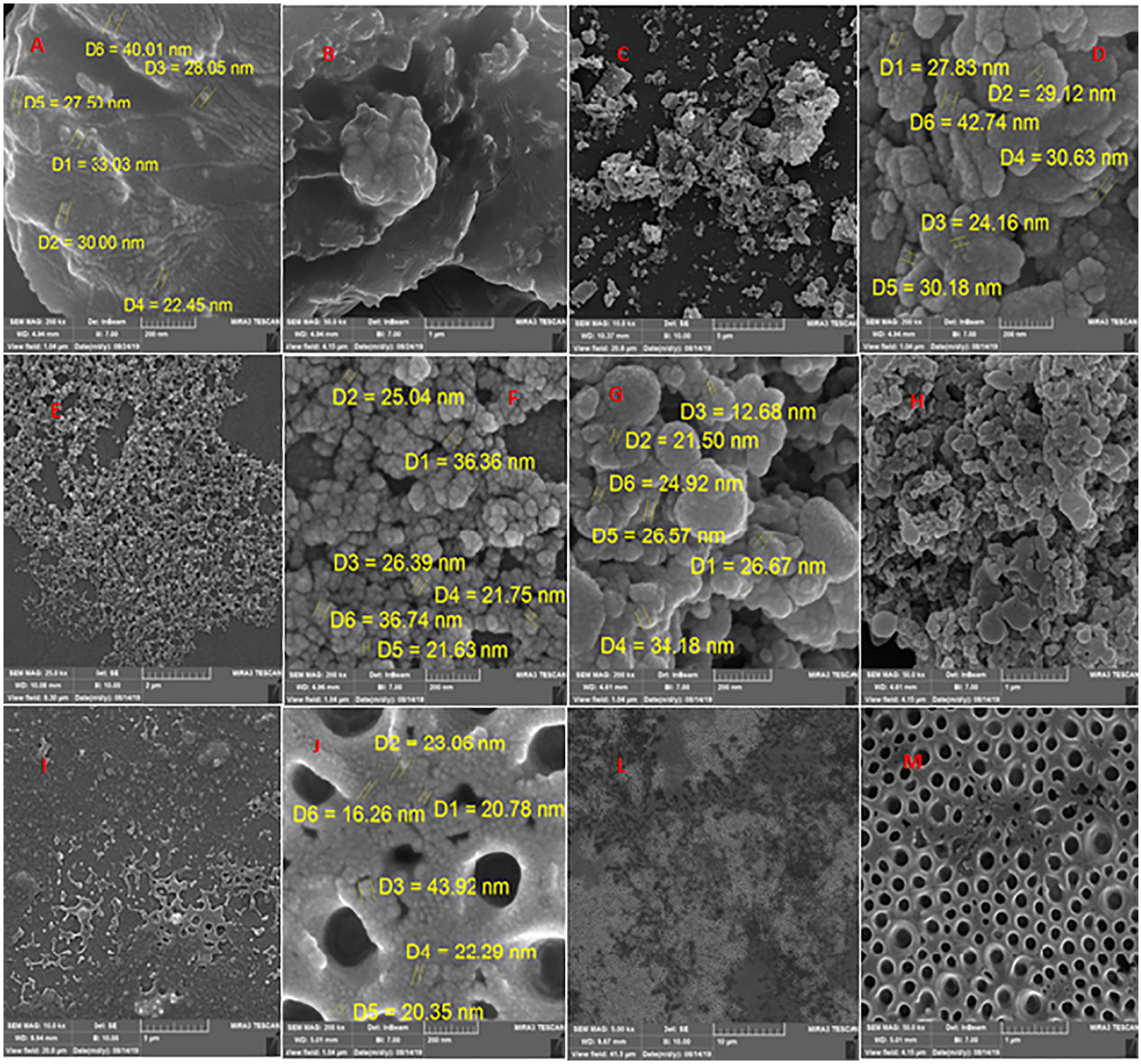

Fig. 3. FE-SEM images of (A–B) bulk Ag-DPA-GQDs nano-ink; (C–D) Ag-DPA-GQDs nano-ink deposited GCE; (E–F) CysA-Au NPs modified Ag-DPA-GQDs nano-ink deposited on the surface of GCE (CysA-Au NPs/Ag-DPA-GQDs/GCE); (G to I) pDNA casted on the surface of CysA-Au NPs/Ag-DPA-GQDs/GCE; and (J to M) cDNA casted on the surface of pDNA/CysA-Au NPs/Ag-DPA-GQDs/GCE.

and as a result of hybridization, the peak current was reduced to 25.82 μA. This indicates that pDNA has successfully immobilized on the substrate.

3.3. Effect of scan rate

Scan rate is one of the important parameters in the study of the electrical activity of different platforms. Therefore, the electrochemical behavior of the CysA-AuNPs/Ag-DPA-GQDs modified GCE in $[Fe(CN)_6]^{3-/4-}$ solutions in the various scan rates from 2 to 1000 mVs^{-1} was evaluated by CV technique (Fig. S5A (see Supporting information)). The linear relationship between the peak current and the sweep rate in the range of 150–1000 mVs^{-1} indicates the mass-transfer was controlled through diffusion process. Depending of Ip *vs* $v^{1/2}$ and ln Ip *vs* ln *v*, are two important factors in evaluating reaction reversibility and whether the reaction is controlled by adsorption or diffusion. These plots are presented for the oxidation peak in Figs. S5 (B and C (see Supporting information)). For irreversible or reversible systems without kinetic complications, Ip varies linearly with $v^{1/2}$, interception the origin. Even though, the plot of I_p on $v^{1/2}$ demonstrated in Fig. S5C (see Supporting information) is linear ($R^2 = 0.9867$), it crosses the origin of axes. In the selected scan rate range from 2 to 1000 mV/s, oxidation peak currents (Ip) depends linearly on square root of the scan rate ($v^{1/2}$) and is explained by the following equation:

$$I_{pa}/\mu A = 65.508\ v(V/s)^{0.5} + 5.2594\ \left(R^2 = 0.9867\right)$$

This dependence does not cross the origin (Fig. S5D (see Supporting information)). This fact can suggest that the electrode process is controlled by diffusion and can be preceded by chemical reaction. On the other hand, a dependence of ln I_{pa} to ln *v* is linear and explained by the following equation:

$$\text{Ln}\ I_{pa}/\mu A = 0.4457\ \text{Ln}\ v(V/s) + 4.2846\ \left(R^2 = 0.9899\right)$$

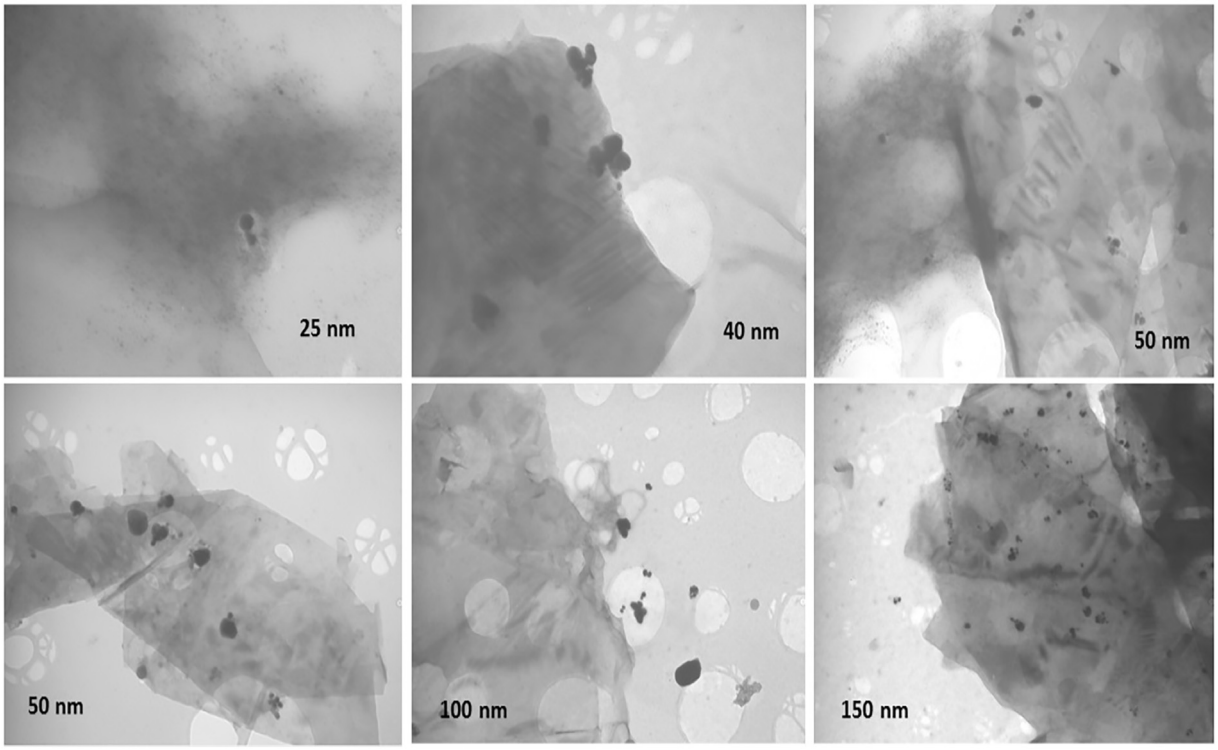

Fig. 4. TEM images of Ag-DPA-GQDs nano-ink in various nano-scales.

Its slope is 0.4457 and show diffusion-control of the electrode process. A slope close to 0.5 and 1 is related to process control with diffusion and adsorption, respectively [36,37].

In irreversible electrochemical reactions, the E_{pa} is independent on v. Since Epa increases as a result of the increase in v, it can be concluded that the reaction is irreversible (Fig. S5E (see Supporting information)).

3.4. Optimization of TB incubation time

Since the incubation time with TB is very significant in DNA probe labeling, the best possible time for labeling was obtained by incubation at 2, 5, 7, 10, and 15 min using SWV techniques in $[Fe(CN)_6]^{3-/4-}$ solution as supporting electrolyte. As can be seen in Fig. 6, the optimum time for incubation with TB is 7 min.

3.5. Optimization of hybridization time

Obtaining the optimum time for hybridization is crucial in evaluating the performance of an engineered genosensor. Hence, different incubation times were investigated. Thus, 10 μL of cDNA was immobilized onto the surface of the biosensor and incubated for 10, 20, 30, 40 and 60 min at 37 °C. Then, the SWV technique was used to obtain the optimum hybridization time. According to the results presented in Fig. 7, the optimal time for pDNA hybridization with cDNA is 30 min.

Table 1
Roughness analysis of AFM images.

R_a (nm)	Window dimensions (micron)	
3.37	1	GQD
1.20	5	GQD
1.39	10	GQD
0.352	1	DPA-GQD
0.482	5	DPA-GQD
11.3	10	DPA-GQD

3.6. Analytical approach

Genosensor sensitivity testing is a critical factor in evaluating the performance of DNA-based sensors. Therefore, the rate of hybridization was assessed by incubating different concentrations of cDNA at 37 °C for 30 min. The results of SWV at concentrations of cDNA (10^{-6}, 10^{-9}, 10^{-12}, 10^{-15}, 10^{-17}, and 10^{-21} M) are presented in Fig. 8. The results showed that by decreasing the concentration of cDNA, the peak current

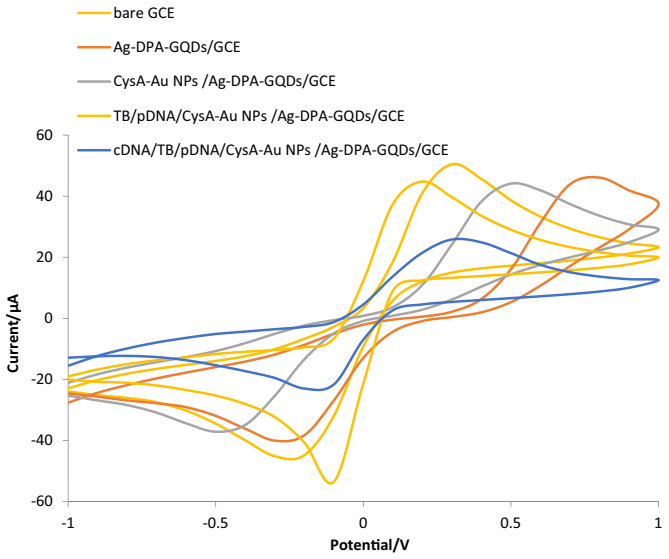

Fig. 5. CVs of bare GCE, DPA-GQDs/GCE, CysA-Au NPs/Ag-DPA-GQDs/GCE, TB/pDNA/CysA-AuNPs/Ag-DPA-GQDs/GCE, and cDNA/TB/pDNA/CysA-Au NPs/Ag-DPA-GQDs/GCE in $[Fe(CN)_6]^{3-/4-}$ (supporting electrolyte). Scan rate is 100 mV/s and potential range is −1 to +1 V.

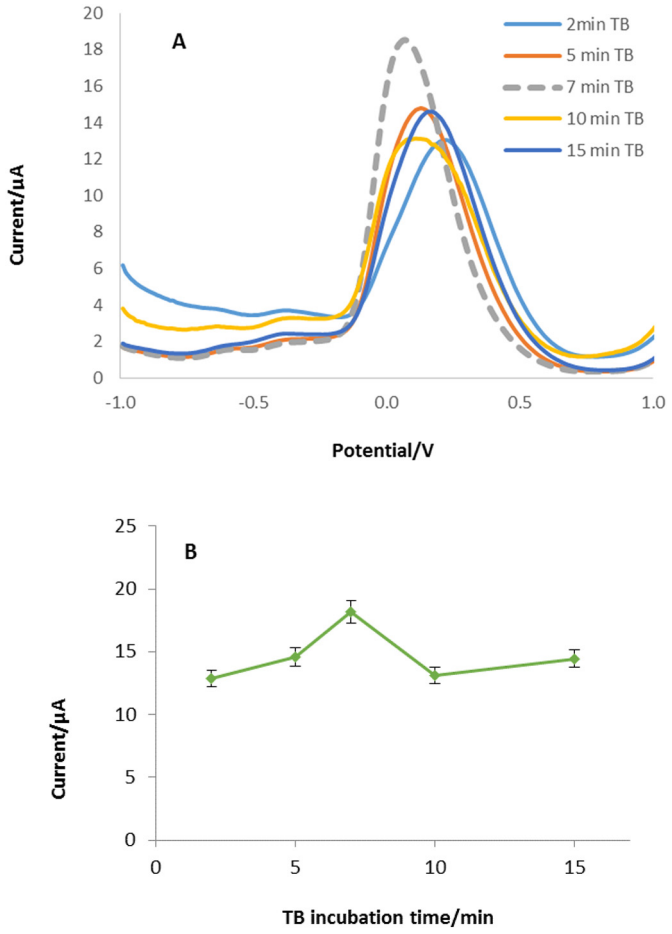

Fig. 6. (A) SWVs of the biosensor after incubation with TB in different times (2, 5, 7, 10, and 15 min). Supporting electrolyte; $[Fe(CN)_6]^{3-/4-}$, TB and pDNA concentration is 20 μM and 100 μM, respectively. (B) Histogram of TB incubation time. $t_{eq} = 2$, $E_{being} = -1$ V, $E_{end} = 1$ V, $E_{step} = 0.1$ V, Amplitude = 0.001 V, frequency = 10 Hz.

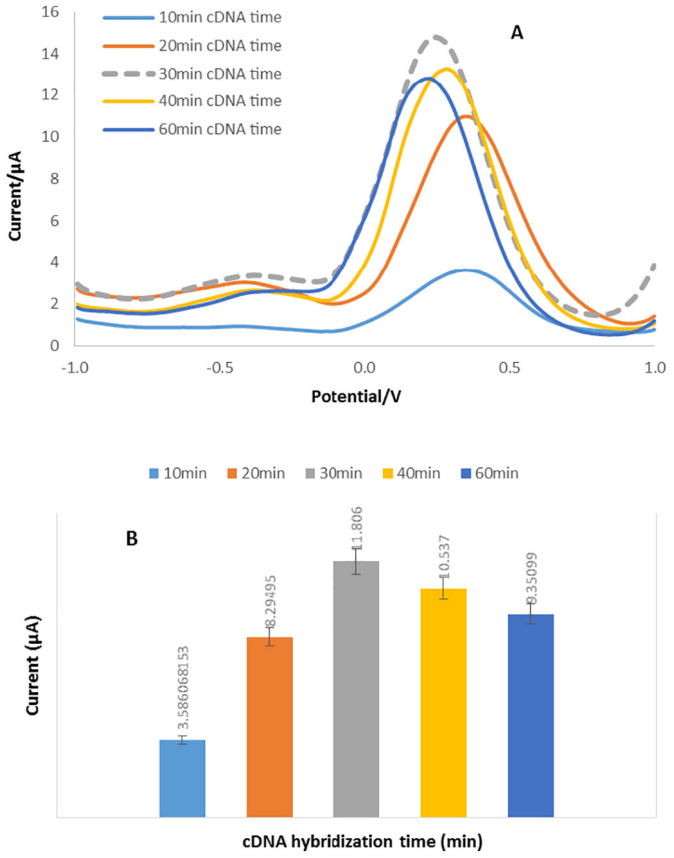

Fig. 7. (A) SWVs of the biosensor after incubation with cDNA in different times (10, 20, 30, 40 and 60 min). Supporting electrolyte; $[Fe(CN)_6]^{3-/4-}$, TB and pDNA concentration is 20 μM and 100 μM, respectively. (B) Histogram of cDNA incubation time. $t_{eq} = 2$, $E_{being} = -1$ V, $E_{end} = 1$ V, $E_{step} = 0.1$ V, Amplitude = 0.001 V, frequency = 10 Hz.

increased. At the optimum conditions, linear range was 1 pM to 1 ZM and low limit of quantification (LLOQ) was 1 ZM. The results of this study are compared with other *H. influenza* detection techniques in Table 2. The results show that the engineered genosensor provides a suitable substrate for detecting influenza at low concentrations. Comparison of the analytical performance of the proposed genosensor with the previous reports show that, this biodevice has better sensitivity than others. Also, there is no need to use of PCR for the pre-treatment of DNA genome before detection. Also, short time of analysis is another advantage of this biosensor. On the other hand, LLOQ is lower than other reports. Based on the results, it can be concluded that this platform promisingly has the potential to be used in diagnosis of *H. Influenza* in clinical samples. The designed biosensor also showed high capability of discriminating one-base, two-base and three-base mismatched sequences. Therefore, a selective biodevice for detection of *H. Influenza* in the presence of negative control was prepared in this research. Also, the prepared genosensor could be easily regenerated and reused to evaluate hybridization process. There are several methods to diagnose H. influenza, including culture, LAT (latex particle agglutination), and PCR (Polymerase chain reaction). The culture and LAT methods are commonly used for the clinical diagnosis of the virus. But, since the *H. influenza* is a fastidious bacterium, growing it requires complex nutrition. Also, replication of these viruses is time-consuming and may take several days or weeks. PRC is more sensitive and specific than previous methods, but it also has disadvantages. Therefore, due to the disadvantages of old methods such as time-consuming, low specificity and sensitivity, the need for specialized people, advanced and expensive equipment, new methods including biosensors have been developed for detection of this virus. Genosensors are alternative and excellent candidate to detection of this virus based on in-direct detection method and monitoring of infectious diseases.

3.7. Genosensor selectivity

At this stage, the selectivity of the designed genosensor was evaluated using the mismatch DNA sequences. For this purpose, after preparation of the biosensor, the mismatch sequences (5′-ATG GAG GTG AAA AAG TTG GAA AAT T-3′, 5′-AGG GAG GTG AAA AAG TTG GAA AAT T-3′, 5′-AGG GAG GTG AGA AAG TTG GAA AAT T-3′) were immobilized on the surface of biosensor and incubated at 37 °C. Then, selectivity of the genosensor to detect similar sequences of DNA was investigated by SWV technique. As can be seen in Fig. S6 (see Supporting information), the peak current in the case of cDNA sequence (5′-ATG CAG GTG AAA AAG TTG GAA AAT T-3′) is higher than the other non-complementary oligonucleotide sequences due to the complete and effective cDNA hybridization. The results show the selectivity and differentiation of the engineered genosensor for detection of cDNA hybridization in comparison with the mismatch target sequence.

3.8. Reproducibility and stability

Two important factors to study in the performance of the sensor are stability and reproducibility. Also, the stability of the probe on the platform surface is significant in the development of DNA-based biosensors [42]. The pDNA/CysA-AuNPs/Ag-DPA-GQDs reproducibility was assessed by keeping it in refrigerator for 7 consecutive days and recording SWVs. The electrochemical behavior of the

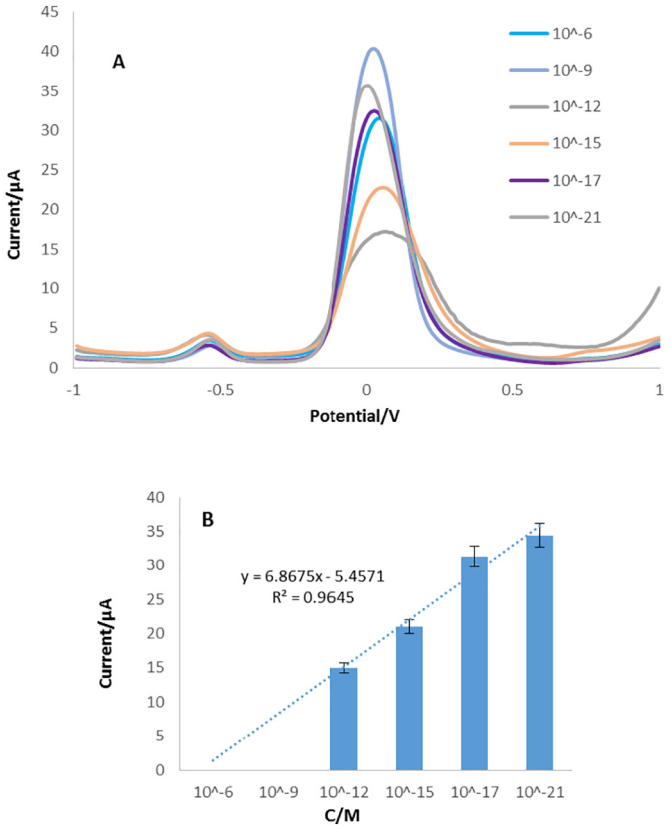

Fig. 8. (A) SWVs of the engineered genosensor in various concentrations of cDNA include: 10^{-6}, 10^{-9}, 10^{-12}, 10^{-15}, 10^{-17}, 10^{-21} M in $[Fe(CN)_6]^{3-/4-}$. (B) Calibration curve of the genosensor. $t_{eq} = 2$, E being $= -1$ V, $E_{end} = 1$ V, $E_{step} = 0.1$ V, Amplitude $= 0.001$ V, frequency $= 10$ Hz.

proposed biosensor in supporting electrolyte indicates that there is a significant difference between the first day current and the other days. Therefore, it can be concluded that this sensor performs best on the first day and its performance decreases day by day (Fig. S7 (see Supporting information)).

3.9. Genosensor response in human plasma samples

Based on the results, engineered genosensor is capable to detection of *H. influenzae* in human plasma samples. For this purpose, the plasma sample was mixed with cDNA 1:1 (v/v) and immobilized on the surface of pDNA/CysA-AuNPs/Ag-DPA-GQDs/GCE. Therefore, a SWV technique was used to detect *H. Influenzae* at different concentrations of cDNA in the plasma sample. The results presented in Fig. S8 (see Supporting information) and show that a decrease in the concentration of cDNA leads to a decrease in the peak current. Using SWV technique, the linear range for unprocessed human plasma without any pretreatment was 1 pM to 1 ZM. In addition, the low limit of quantification LLOQ was 1 ZM.

3.10. Regeneration of the genosensor

Reusability of DNA-based biosensors is essential for continuous detection of target samples. In this work, DNA-based biosensor regeneration was investigated by incubation at 60 °C for 5 min. In this way, after the first hybridization and recording of SWV, this biosensor was incubated at 60 °C and re-hybridization was performed. So, SWV was recorded. It was observed that the biosensor performance in the second hybridization significantly decreased compared to the first hybridization (Fig. S9 (see Supporting information)). It seems that the decrease in current is due to the loss of CysA/AuNPs and thiolated pDNAs on the electrode surface. Therefore, this biosensor has no ability to regeneration and this is a failure for ink-based biosensors.

4. Conclusion

In summary, a new DNA-based electrochemical biosensor for rapid and sensitive detection of *H. influenza* in human plasma samples was developed. For this purpose, a unique conductive nano-ink based on silver nanoparticle-D-penicillamine functionalized grapheme quantum dots (Ag/DPA-GQDs) was synthesized. The morphology of the particles in bulk ink solution was investigated using TEM and SEM. DPA-GQDs needed for ink production was also identified after synthesis by various methods including AFM, FTIR, and DLS. The Ag/DPA-GQDs nano-ink was electrodeposited on the surface of GCE and followed by electrodeposition of CysA/AuNPs. Subsequently, the primer was immobilized on the surface of CysA/AuNPs/Ag/DPA-GQDs/GCE. Finally, the designed genosensor was used to detection of DNA hybridization. Using SWV technique and under the optimized conditions, the low limit of quantitation (LLOQ) for the proposed genosensor was recorded as 1 ZM, which this evaluation was performed at highly linear range of 1 pM to 1 ZM. Based on the results, it can be concluded that this platform promisingly has the potential to be used in diagnosis of *H. Influenzae* in clinical samples.

Supplementary data to this article can be found online at https://doi.org/10.1016/j.ijbiomac.2020.02.062.

CRediT authorship contribution statement

Arezoo Saadati: Writing - original draft. **Soodabeh Hassanpour:** Writing - original draft. **Mohammad Hasanzadeh:** Conceptualization, Writing - original draft, Writing - review & editing. **Nasrin Shadjou:** Conceptualization, Writing - original draft, Writing - review & editing.

Declaration of competing interest

All the authors (A. Saadati, S. Hassanpour, M. Hasanzadeh and N. shadjou) have read, approved and made substantial contributions for the manuscript. None of the original material contained in this manuscript has been previously published nor is currently under review for publication elsewhere. Besides, authors declare no conflict of interests and/or commercial products or companies.

Table 2
Analytical figure of merit for detection of Haemophilus influenza.

Detection methods	Materials	Linear range	LOD and LLOQ	Ref.
DNA-based biosensor	CTAB/AuNPs	1 μM to 1 ZM	1 ZM	[9]
Immunosensor	RGO	1 to 104 PFU mL^{-1}	0.5 PFU mL^{-1}	[38]
Real-time PCR	–	1 to 10^6 organisms per reaction mixture	–	[39]
Duplex quantitative PCR	–	–	0.0125 pg	[40]
Quantitative real-time PCR	–	–	10^4 DNA copies/mL	[41]
DNA-based biosensor	Ag-DPA-GQDs nano-ink/CysA-Au NPs	1 pM to 1 ZM	1 ZM	This work

Acknowledgements

This research work was supported by Tabriz University of Medical Sciences.

References

[1] K.M. Millan, S.R. Mikkelsen, Anal. Chem. 65 (1993) 2317–2323.
[2] K. Kerman, Y. Morita, Y. Takamura, E. Tamiya, Anal. Bioanal. Chem. 381 (2005) 1114–1121.
[3] K.-F. Low, A. Karimah, C.Y. Yean, Biosens. Bioelectron. 47 (2013) 38–44.
[4] Q. Sheng, J. Wang, J. Zheng, Z. Xu, H. Zhang, Biosens. Bioelectron. 25 (2010) 2071–2077.
[5] L. Dai Tran, B.H. Nguyen, N. Van Hieu, H.V. Tran, H. Le Nguyen, P.X. Nguyen, Mater. Sci. Eng. C 31 (2011) 477–485.
[6] V. Perumal, U. Hashim, S.C. Gopinath, R. Haarindraprasad, K. Foo, S. Balakrishnan, P. Poopalan, Sci. Rep. 5 (2015), 12231.
[7] A. Miodek, N. Mejri, M. Gomgnimbou, C. Sola, H. Korri-Youssoufi, Anal. Chem. 87 (2015) 9257–9264.
[8] N. Oliveira, E. Souza, D. Ferreira, D. Zanforlin, W. Bezerra, M. Borba, M. Arruda, K. Lopes, G. Nascimento, D. Martins, Sensors 15 (2015) 15562–15577.
[9] S. Hassanpour, A. Saadati, M. Hasanzadeh, Int. J. Biol. Macromol. 180 (2020), 113050.
[10] J.R. Gilsdorf, C.F. Marrs, B. Foxman, Infect. Immun. 72 (2004) 2457–2461.
[11] M.P. Slack, H.J. Azzopardi, R.M. Hargreaves, M.E. RAMSAY, Pediatr. Infect. Dis. J. 17 (1998) S204–S207.
[12] P.D. Butler, E.R. Moxon, Microbiology 136 (1990) 2333–2342.
[13] J. Puri, V. Talwar, M. Juneja, K. Agarwal, H. Gupta, Indian Pediatr. 36 (1999) 1029–1031.
[14] W. Kennedy, S. Chang, K. Purdy, T. Le, P. Kilgore, J. Kim, D. Anh, P. Huong, B. Dong, D. Tan, Epidemiol. Infect. 135 (2007) 1217–1226.
[15] A. Mobed, M. Hasanzadeh, M. Agazadeh, A. Mokhtarzadeh, M.A. Rezaee, J. Sadegi, Int. J. Biol. Macromol. 121 (2019) 1295–1307.
[16] M.L. Yola, T. Eren, N. Atar, Electrochim. Acta 125 (2014) 38–47.
[17] M. H. Abdalhai, A. n. M. Fernandes, X. Xia, A. Musa, J. Ji and X. Sun, J. Agric. Food Chem., 2015, 63, 5017–5025.
[18] S. Dash, A. Kumar, J. Bacteriol. Mycol. Open Access 4 (2017), 00095.
[19] A. Ulianas, L.Y. Heng, M. Ahmad, H.-Y. Lau, Z. Ishak, T.L. Ling, Sensors Actuators B Chem. 190 (2014) 694–701.
[20] A. Chaubey, B. Malhotra, Biosens. Bioelectron. 17 (2002) 441–456.
[21] R. Das, M.K. Sharma, V.K. Rao, B. Bhattacharya, I. Garg, V. Venkatesh, S. Upadhyay, J. Biotechnol. 188 (2014) 9–16.
[22] M. Wu, X. Xu, J. Wang, L. Li, ACS Appl. Mater. Interfaces 7 (15) (2015) 8243–8250.
[23] F. He, L. Liu, L. Li, Adv. Funct. Mater. 21 (2011) 3143–3149.
[24] T. Ramulu, R. Venu, B. Sinha, B. Lim, S. Jeon, S. Yoon, C. Kim, Biosens. Bioelectron. 40 (2013) 258–264.
[25] L. Wang, X. Chen, X. Wang, X. Han, S. Liu, C. Zhao, Biosens. Bioelectron. 30 (2011) 151–157.
[26] M. Lütfi Yola, N. Atar, Appl. Surf. Sci. 458 (2018) 648–655.
[27] M. Lütfi Yola, N. Atar, J. Electrochem. Soc. 165 (2) (2018) H1–H9.
[28] O. Akyıldırım, F. Kardaş, M. Beytur, H. Yüksek, N. Atar, M.L. Yola, J. Mol. Liq. 243 (2017) 677–681.
[29] M. Lütfi Yola, N. Atar, J. Electrochem. Soc. 164 (6) (2017) B223–B229.
[30] M. Lütfi Yola, N. Atar, J. Electrochem. Soc. 163 (14) (2016) B718–B725.
[31] A. Tolga Çolak, T. Eren, M. Lütfi Yola, E. Beşli, O. Şahin, N. Atar, J. Electrochem. Soc. 163 (10) (2016) F1237–F1244.
[32] S. Hassanpour, A. Saadati, M. Hasanzadeh, N. Shadjou, A. Mirzaie, A. Jouyban, Microchem. J. 145 (2019) 266–272.
[33] S. Hassanpour, A. Saadati, M. Hasanzadeh, J. Pharm. Biomed. Anal. 180 (2020) 113050.
[34] A. Mobed, M. Hasanzadeh, N. Shadjou, S. Hassanpour, A. Saadati, M. Aghazadeh, Microchem. J. 152 (2020), 104286.
[35] S. Wang, H. Xin, J. Phys. Chem. B 104 (2000) 5681–5685.
[36] P. Kissinger and W. R. Heineman, Laboratory Techniques in Electroanalytical Chemistry, Revised and Expanded, CRC Press, 1996.
[37] L.R. Faulkner, A.J. Bard, Electrochemical Methods: Fundamentals and Applications, John Wiley and Sons, 2002.
[38] R. Singh, S. Hong, J. Jang, Sci. Rep. 7 (2017), 42771.
[39] A. Marty, O. Greiner, P.J. Day, S. Gunziger, K. Mühlemann, D. Nadal, J. Clin. Microbiol. 42 (2004) 3813–3815.
[40] C. De Gier, J.L. Pickering, P.C. Richmond, R.B. Thornton, L.-A.S. Kirkham, J. Clin. Microbiol. 54 (2016) 2380–2383.
[41] G.M. Abdeldaim, K. Strålin, L.A. Kirsebom, P. Olcén, J. Blomberg, B. Herrmann, Diagn. Microbiol. Infect. Dis. 64 (2009) 366–373.
[42] A. Liu, K. Wang, S. Weng, Y. Lei, L. Lin, W. Chen, X. Lin, Y. Chen, TrAC Trends Anal. Chem. 37 (2012) 101–111.